Design, Manufacture and Application of In-board Magnetic Devices

Yi E. Zhang
Edwin.zhang@vishay.com
Vishay Siliconix Corporation
2201 Laurelwood Rd
Santa Clara, CA 95054 U.S.A.
Tel: 1-408-567-8233
Fax: 1-408-567-8147

Seth R. Sanders
sanders@eecs.berkeley.edu
Department of Electrical Engineering and Computer Sciences
University of California, Berkeley
Berkeley, CA 94720 U.S.A.
Tel: (510)-642-4425
Fax: (510)-642-2739

Abstract: Transformers and inductors can be integrated within a multilayer printed circuit board as described in [1]. These devices offer great advantages in packaging density. The planar type form factor provides for a large surface area to volume ratio, allowing for effective heat transfer from the magnetic device.

This paper takes a tilt factor for winding resistances into consideration, and develops a more accurate design methodology for in-board magnetic devices. Manufacture challenges includes burying of magnetic cores, controlling internal stress and plating through deep vias. A propose manufacture process is described in detail. Finally a transformer and an inductor were designed for an example dc-dc converter demonstrating the manufacturability of in-board magnetic devices. Measured parameters match fairly well with the simple models.

1. Introduction

Higher power density and higher efficiency have no doubt been the major trends for power converters. For some applications, a lower profile, which means more power can be converted in a given volume, is also preferred. Power magnetic devices need to fit these trends.

Wire-wound transformers and inductors are bulk and have high profiles. Their repeatability is also poor. Large design rooms have to be left to tolerant the parasite variations. The Planar magnetic structures [2]-[6] have been studied extensively for the last few years, and there have been efforts [7]-[8] to combine transformers and inductors on the same core so that the total magnetic volume is reduced.

The planar winding structure is more reliable, the profiles can be much lower, and the cost can be lower for large quantity orders as the manual processes for making windings are eliminated.

However, this structure is usually still the one that has the highest profile on the board. The only way to reduce the profiles of the magnetic devices further is to reduce the height of the cores on both sides of the print circuit board. To keep the same cross-section, the cores have to be wider and cover more board space. As the surface area covered by the cores cannot be used for surface mounted devices, it limits the possibility to further reduce the profile and increase the power density. Also, as the copper utilization is low for spiral windings, usually only one or two turns can be laid on each PCB layer, especially for high current windings. For a design that requires a lot of turns, the number of PCB laminations has to increase, which leads to an increase in cost. A new way to connect multilayer boards and two layer boards has been invented recently. With this technology, only the magnetic devices need to be made on multilayer boards, the rest of the converter can be laid on a two-layer board. This method may lower the cost, but the real state occupied by the magnetic devices still can not be used for other surface mounted devices.

There has been a lot of research [8]-[14] toward building magnetic devices on wafers. The goal is to make the whole dc/dc converter on a single chip. It has been shown that these micro-fabricated magnetic devices have the potential to have very high power density with a decent efficiency. Even though we believe this is possibly the future of power electronics, so far there are still some hurdles.

The IC process has the potential to reduce the cost for mass productions, but magnetic cores usually require none standard IC processes. A more likely solution is to make the magnetic devices separately from the rest of the circuits, and connect them with multi-chip technology. As ferrite cores are not compatible with IC processes, usually laminations of metal cores are used for microfabrication. Lamination processes significantly increase the cost of the magnetic devices. To save process time and cost, the lamination stack cannot be very thick, and these devices are usually optimized around the frequency of 1-30 MHz. At these frequencies,

switching devices have very high losses. Skin effect and proximity effect can also be a serious problem for high current applications. So even though we can make excellent integrated magnetic devices optimized in the MHz range, the whole converter will have very low efficiency at these frequencies.

Reference [1] introduces a design and prototyping process for integrating magnetic components, transformers and inductors, within a multilayer printed circuit board (PCB). The advantages of the in-board magnetic devices include low profile, more effective heat transferring and the surface real estate is fully available for other surface mountable components.

In this paper, a more detailed design methodology is developed. It also describes the manufacture challenges, and introduces a propose solution. Finally, a 100W 48V/3.3V DC-DC converter is built demonstrating the manufacturability of the in board magnetic devices.

2. Tilt factor for winding resistance

The resistance for radial current flow in an annular shape winding (1 turn, 2 sides) is

$$R_1 = 2\int_{r_1}^{r_2} \frac{\rho_{cu}}{2\pi r h_c} dr = \frac{\rho_{cu}}{\pi h_c} \ln(\frac{r_2}{r_1}) \qquad (1)$$

where ρ_{cu} is the resistivity of the copper, hc is the height of the copper, r_1 and r_2 are inner and outer radii of the winding respectively. Dividing the above winding into N turns, the width of the winding decreased by N, and the length increases by N. Thus, the resistance is increased by a factor of N^2, yielding

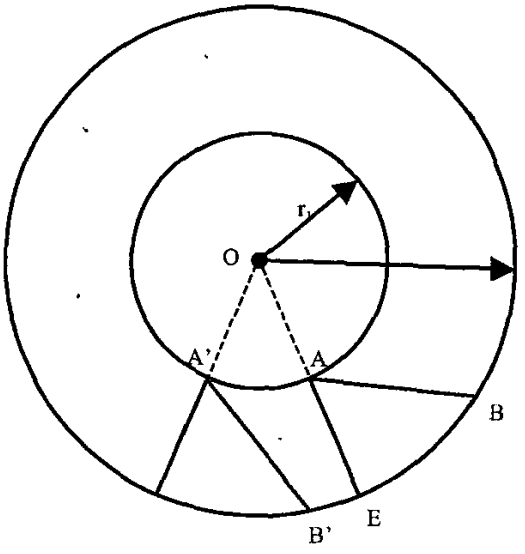

Fig.1. Tilted (trace A'B'BA) and un-tilted (trace A'E'EA) winding traces

$$R_N = \frac{N^2 \rho_{cu}}{\pi h_c} \ln(\frac{r_2}{r_1}) \qquad (2)$$

Equation (2) is used for transformer and inductor winding resistance calculations in reference [1]. Here we assumed the direction of each copper trace is purely radial, like trace A'E'EA in Fig. 1. In other words, if we extend the two side edges (AE and A'E') of the trace, they merge at center O. In reality, each trace, like trace A'B'BA shown in Fig.1, must be tilted toward the azimuthal direction to finish a toroidal current loop. Compared with trace A'E'EA, trace A'B'BA is longer, and the effective width turns out to be smaller as well. Both factors boost the winding resistance. A tilt factor can be defined as the ratio of tilted and un-tilted winding resistances.

Assume a winding starts at one point on the core. After each n turns, the winding goes azimuthally around the core and comes back to the original point. Appendix 1 proves that the tilt factor is approximately:

$$F_{tilt} = \ln(\frac{r_2 \sin(\theta_1 + \frac{\pi}{n})}{r_1 \sin\theta_1}) / \ln(\frac{r_2}{r_1}), \qquad (3)$$

where θ_1 can be calculated by

$$\tan\theta_1 = (\cos\frac{\pi}{n} - \frac{r_1}{r_2}) \cdot \frac{1}{\sin(\pi/n)}. \qquad (4)$$

The tilt factor F_{tilt} is a measurement of how much winding resistance is increased because of the tilt of the traces. From (3) and (4), the tilt factor is a function of r_1/r_2 and number of turns n. As shown in Fig.2, the tilt factor increases rapidly as the inner radius of the trace (r_1) gets close to the outer radius of the trace (r_2). The tilt factor also increases as number of turns n increases.

According to [1], for a transformer with a ring shape core, the core loss is approximately proportional to, while the copper loss is approximately inversely proportional to $N_2^2 \ln(\frac{r_3}{r_1})$, where N_2 is the number of secondary turns. Decreasing the number of turns or increasing the ratio of r1/r2 causes the copper loss to decrease and core loss to increase. A minimum total loss design is usually reached while copper and copper loss are balanced. Now if the number of turns is too small and/or inner and outer radii of the windings are too close, the tilt factor kicks in, and causes the winding resistance increase significantly. Taking the tilt factor into consideration tends to give optimal designs with less number of turns or smaller ratio for inner and outer winding radii.

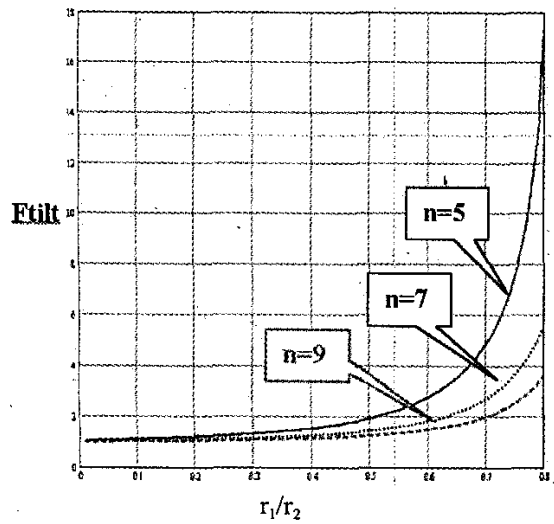

Fig. 2. Tilt factor as a function of ratio of inner and outer radius and number of turns N

3. Manufacture

The processes for in-board magnetic devices are similar to the standard multi-layer buried via processes. However, there are two major differences or challenges. First, magnetic cores have to be buried inside the printed circuit board, and second, as the buried cores increase the depth of vias, copper platting in the deep vias can also be an issue.

Fig. 3 shows the outline of the manufacture processes. Three pressing-plating cycles are needed.

Step 1: Prepare the core PCB and bury the magnetic cores

Slots for the magnetic cores are first cut in the core PCB. Proper assembling spaces are critical for a successful lamination. The spaces should be large enough to make the core assembly feasible, and also large enough to allow for the different temperature

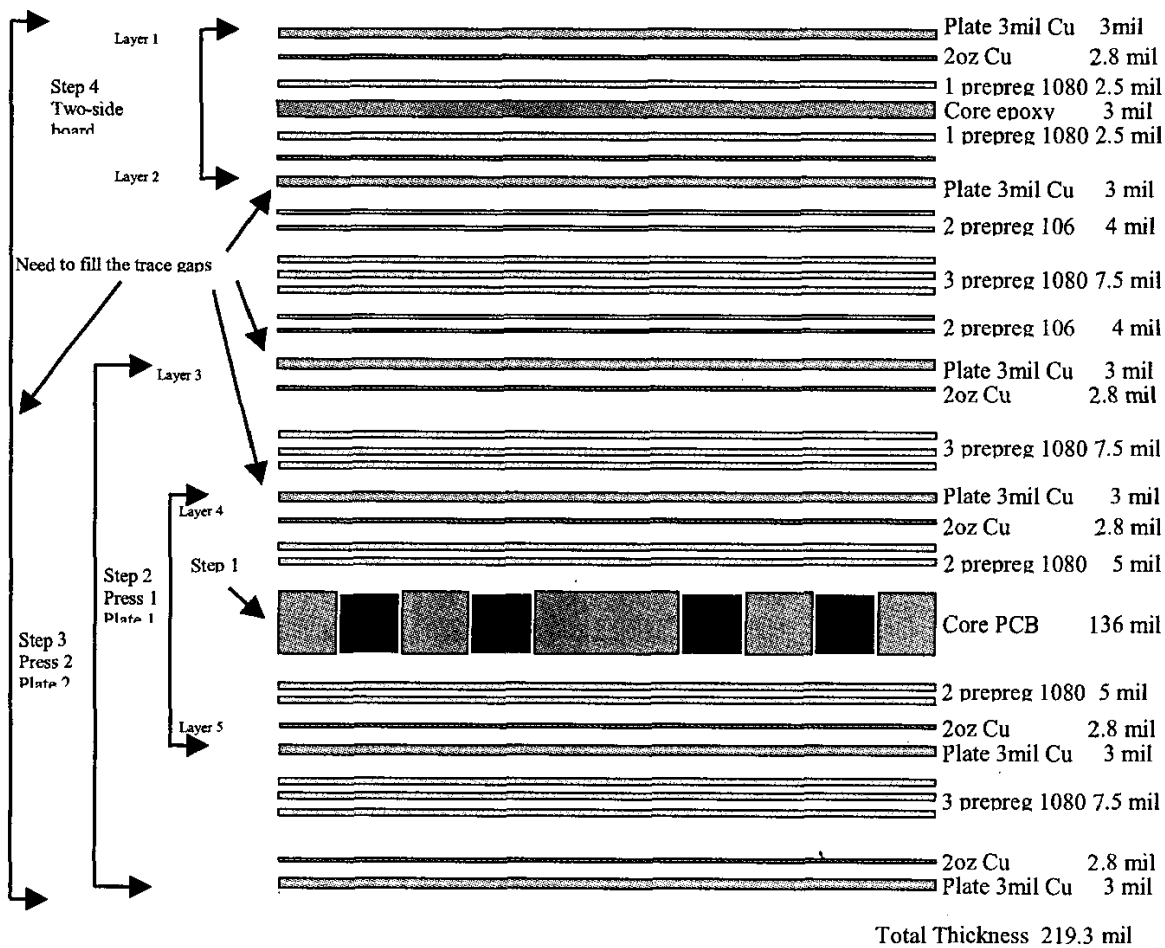

Fig. 3 In-board magnetic processes (vias are not shown)

coefficients of the magnetic core and core PCB materials. A gap of 0.005 inches was used for all the spaces.

Step 2: The first pressing-plating cycle

Next, as shown in Fig. 3, two prepreg layers with 2-oz copper foils are added on each side of the core PCB with embedded magnetic cores, and a subsequent pressing cycle is done in a vacuum camber, which avoids air bubbles in the intermediary spaces.

Note that the core epoxy must be a little bit (about 0.01 inches in our design) thicker than the magnetic cores, otherwise, most of the pressure during pressing may be put onto the magnetic cores. Ferrite cores may crack and/or undergo change of their magnetic properties. Metal based, tape-wound cores like Metglas cores do not crack, but may change magnetic properties under pressure.

During the pressing cycle, the board is subjected to heat and pressure that melts the B-stage (sticker sheets or prepregs) and causes it to flow. The process involves B-stage melt, flow, cure and cool steps. The pressing cycles start with a low pressure as a "kiss" pressure. The "kiss" pressure is high enough to assure good thermal contact without damaging the muti-layer boards. Full pressure is applied during the flow and cure steps, and a portion of the cool steps. For a standard epoxy system, heating rates are between 5-20°C/min in the melt and flow steps, while cooling rate at cool step can be even higher; a maximum temperature (usually170-180°C) is held for 60-90 min. during the cure step. Because of the pressure on the magnetic cores, lower heating and cooling rates (~1-2°C/min) are preferred to avoid internal stress, and longer cure times (3~4 hours) are needed to make sure all volatiles are removed. The temperature and pressure profiles are also plotted on Fig. 4.

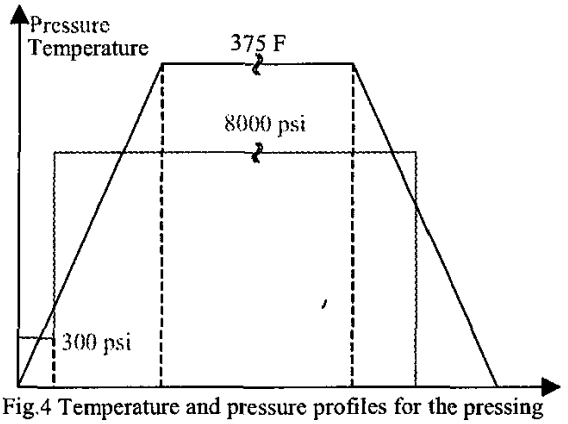

Fig.4 Temperature and pressure profiles for the pressing cycles

Following the first pressing cycle is the standard buried via process. Vias are first drilled, and 2-oz copper is plated both on the board surfaces and on the walls of all the vias, and the required pattern is acquired by the etching process. Up to this point, one of the transformer/inductor windings is finished

Step 3: Second pressing-plating cycle (standard)

There is no need to do the second pressing cycle in the vacuum camber. Otherwise, this step is just a repeat of step 2. The transformer and the inductor are finished at the end of this step.

Step 4: A separate two-sided board is made for the remaining parts of the converter, excluding the magnetic devices.

Step 5: Third pressing–plating cycle

Finally a third standard pressing-plating cycle (repeat of step 3) is required to make the connection between the magnetic devices and the remainder of the converter.

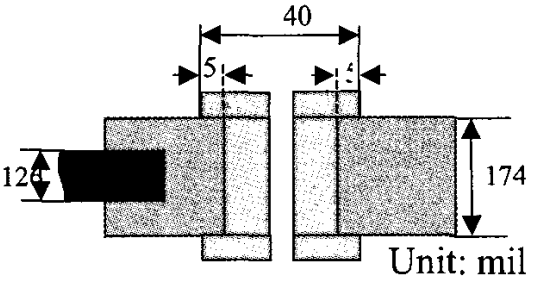

Fig. 5. Plating through the deep via

Fig. 5 shows the cross-section of a deep via in our sample design. The sizes of the vias should be chosen according to the manufacturing capability and the depths of the vias. The ratio between the depth of a via to the smallest size (diameter) of the via is called the aspect ratio. Most of the PCB manufacturers can realize an aspect ratio less than seven [16]. State of the art technologies can plate vias with aspect ratio as high as sixteen. As relatively thick (2-oz) copper are platted in the vias, to be on the safe side, the via size was chosen to be 0.03 inches, which results in an aspect ratio of 5.8 for the transformer and inductor part. Bigger via sizes can be used for connection between the magnetic devices to the rest of the converter circuits. In the sample design, 0.04 inches vias are used for connection between the signal layer and the magnetic devices, that results in an aspect ratio of about five and still stays within the specifications for most manufacturers.

Anther obvious question is whether converters using in-board magnetic devices can cost less. The answer depends on the application. Fig. 6.5 in reference [16] shows that the cost of the PCB depends mainly on the

number of laminations and minimum feature size. For power converters, dimensions are usually big enough that the minimum feature size is not the dominant cost factor. Then, the PCB cost per unit area is almost proportional to the number of lamination layers. The number of laminations for a planar winding structure is usually decided by the number of turns for a high current transformer or inductor. The in-board magnetic devices require two or four layers. For many applications, in-board magnetic devices probably require less number of laminations. Of course, there are two extra costs for in-board magnetic devices, one is the cost to bury the magnetic cores, the other is to plate through relatively deeper vias, but as far as we know, these costs are not the dominant ones.

4. 100W transformer and inductor with in-board magnetic processes

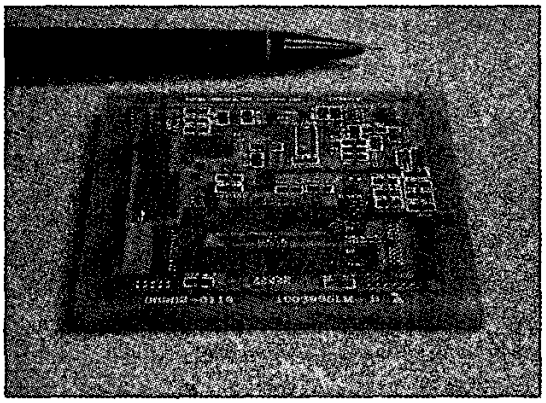

Fig. 6 Prototype of the 100W dc-dc converter with concentric transformer and inductor buried

A 100W transformer and an inductor were designed for a 48V to 3.3V dc-dc converter using active clamp topology. The last section details the manufacturing processes of the six-layer board that realizes the whole dc-dc converter. Fig. 6 shows a sample of such a six-layer board. The top two layers realize the converter interconnections other than those for the transformer and inductor. Ground plane on the second layer effectively shields other parts of the converter from the magnetic field created by the transformer and inductor. These fields have already been significantly reduced by matching the winding dipole fields as discussed in [1] and [13-15].

Fig. 7 shows the cross-section of the six-layer board. We chose to pick rather thick cores to demonstrate the potential of this technology. Reducing the core height to half would only increase the total loss of the magnetic devices by about $\sqrt{2}$ and would make the manufacturing process considerably simpler.

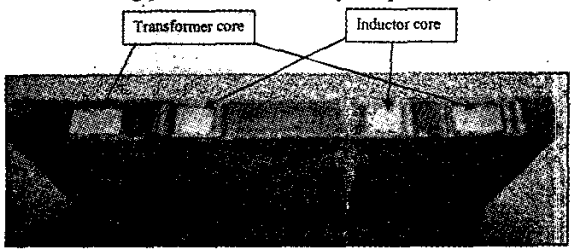

(a) Whole cross-section

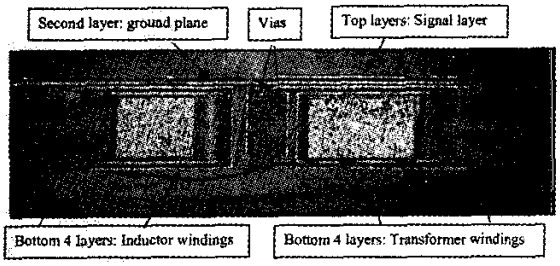

(b) Amplified picture of half of the cross-section

Fig. 7 Cross-section of the 6-layer converter board

Test data taken on the prototype transformer and inductor are shown in Table 1 and 2 respectively. The calculated and measured dc winding resistance values are pretty close. The minor differences can be explained by the unevenness of the spaces between windings. The extra inductor core loss is because of the residue pressure inside the PCB. More spaces should be left for inductor cores.

Table 1. Electrical performance of prototype transformer design

Symbol	Meaning	Calculated	Measured
	DC Primary trace resistance	99mΩ	
	DC Primary via resistance	13.5mΩ	
R_{pri}	DC Primary resistance	112.5mΩ	120mΩ
	DC Secondary trace resistance	1.47mΩ	
	DC Secondary via resistance	0.2mΩ	
R_{sec}	DC Secondary resistance	1.69mΩ	1.92mΩ
L_s	Primary leakage inductance	58 nH	93nH
P_{core}	Core loss	1632mW	1607mW

Symbol	Meaning	Calculated	Measured
R_{in}	Inner winding DC resistance	1.65mΩ	
R_{sec}	Outer winding DC resistance	1.83mΩ	
Rin//Rsec		0.88mΩ	1.16mΩ
P_{core}	Core loss	0.586 W	0.985 W

Table 2 Electrical performance of prototype inductor

Fig. 8 shows the contribution of each of the converter loss terms. The total calculated loss at full load is 15.4 W, and the measured loss is 19.1W. The core loss and copper loss of the inductor are relatively well balanced. Transformer copper loss is much higher. This is because we did not take tilt factor into account for the original design. The unevenness of the spaces between copper traces due to hand layout also increases the winding resistance. The winding loss is somewhat bigger than the *number we used for optimization.*

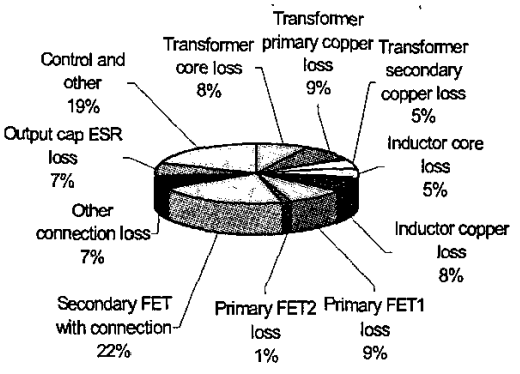

Fig. 8 Contribution of different converter losses

Primary winding to secondary winding	2500V
Primary winding to primary ground	2600V
Primary winding to secondary ground	3600V
Secondary winding to primary ground	2600V
Secondary winding to secondary ground	2500V

Table 3. Measured breakdown voltages from a sample converter

Laying out the primary and secondary windings on different layers of the PCB makes the isolation design feasible. Table 3 listed the measured breakdown voltages from a sample converter.

Obviously, the isolation capability is good enough for many applications. It can be fairly easily adjusted by controlling the minimum space between isolated parts.

Appendix 1. Prove of the formula for tilt factor

From part one, we know each trace must be tilted toward the azimuthal direction as shown in Fig. 9 to finish a toroidal current loop. Assume the middle point of the trace inner arc AA' is A'', and outer arc BB' has a middle point B'', the angle θ_2 (or $\angle$A''OB'') is a measure of how much each trace is tilted in the azimuthal direction. Assume for each n turns, the winding goes azimuthally around the core and comes back to the original point. Then the summation of θ_2 for all the traces is 2π. Since each turn has a top trace and a bottom trace, for each trace,

$$\theta_2 = \frac{2\pi}{2n} = \frac{\pi}{n}. \tag{5}$$

Let us calculate a general formula for resistance of area A'B'BA. Extend A"B", and draw a line OO' perpendicular to A"B". Draw CC' and DD' through A" and B" respectively, and make them both perpendicular to O'B". Make AC and A'C' perpendicular to CC', then CC' is the projection of arc AA' on axis CC'. Similarly, make BD and B'D' perpendicular to DD', and DD' is the projection of arc BB' on axis DD'. Now if we can prove

$$\frac{O'A''}{O'B''} = \frac{CC'}{DD'}, \tag{6}$$

equivalently we have proved that DC and D'C' would merge at O'. Now if we assume C,C',D,D' are very close to A,A',B,B' respectively, then AA' merges with BB' at O'. The area AA'B'B can be approximately seen as a fan-shaped winding centered at O', with inner radius of *OA"* and outer radius of *OB"*.

Now let us prove (6):

Because OA" $\perp$ AA' and O'A" $\perp$ CC',

then $\angle$A'A"C'= $\angle$OA"O'=90°-θ_1.

Also because A'C' $\perp$ A"C',

therefore $\angle$A"A'C'=θ_1.

Assume arc AA' and line AA' have about the same length, then

$$CC' \approx AA' * \sin\theta_1. \tag{7}$$

Similarly,

$\angle$B"B'D'= $\theta_1+\theta_2$,

$$DD' \approx BB' * \sin(\theta_1+\theta_2). \tag{8}$$

If BB' had not been tilted in the azimuthal direction,

$$BB'/AA' = r_2/r_1. \tag{9}$$

After the trace has been tilted in the azimuthal direction, the length of the arc (BB') should be the same. Plug (7) and (8) into (9), we have

$$\frac{CC'}{DD'} = \frac{r_1 \sin\theta_1}{r_2 \sin(\theta_1+\theta_2)} = \frac{O'A''}{O'B''}$$

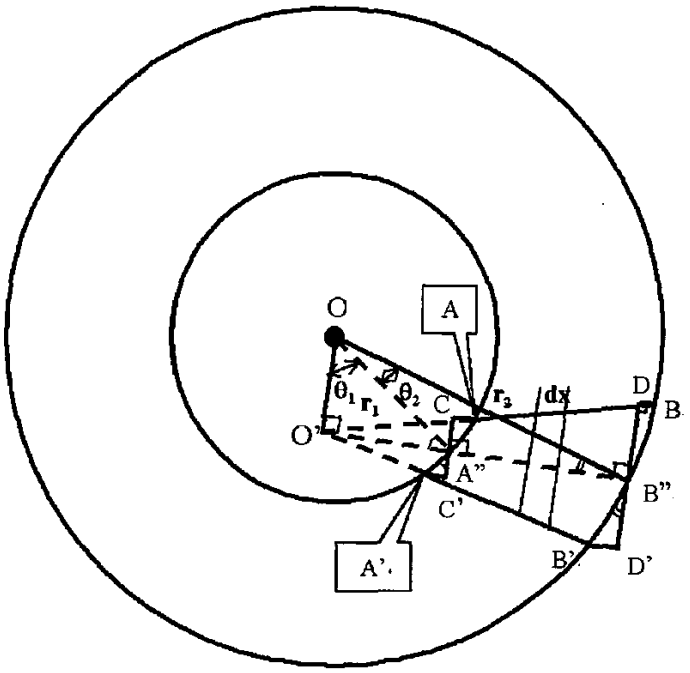

Fig. 9. Winding resistance considering rotating in the azimuthal direction

Now we are ready to approximate the resistance of AA'B'B. In Fig. 9, pick up a section dx and assume the distance from O' to this section is x, then the width of the dx section is

$$W_{dx} \approx \frac{CC'*x}{O'A''}.$$

Resistance of dx section becomes

$$R_{dx} \approx \frac{\rho_{cu} * OA''*dx}{x*CC'*h_c}, \quad (10)$$

where h_c is the thickness of the copper.

As ∠B"O'O = 90°, it is easy to get:

$$O'A'' = r_1 \sin\theta_1 \quad (11)$$

$$O'B'' = r_2 \sin(\theta_1 + \theta_2) \quad (12)$$

$$r_1 \cos\theta_1 = r_2 \cos(\theta_1 + \theta_2)$$

Equivalently

$$\tan\theta_1 = (\cos\theta_2 - \frac{r_1}{r_2}) \cdot \frac{1}{\sin\theta_2}.$$

Inserting (5) in equation above,

$$\tan\theta_1 = (\cos\frac{\pi}{n} - \frac{r_1}{r_2}) \cdot \frac{1}{\sin(\pi/n)}. \quad (13)$$

$$AA' = \frac{2\pi r_1}{N} - s \quad (14)$$

where s is the space between each trace.

Inserting (7), (11), (12) and (14) into (10), we have the integral

$$R_{AABB} \approx \int_{OA'}^{OB''} \frac{\rho_{cu} * OA''}{x*CC'*h_c} dx = \int_{r_1 \sin\theta_1}^{r_2 \sin(\theta_1+\theta_2)} \frac{\rho_{cu} * r_1 \sin\theta_1}{x*AA'*\sin\theta_1 * h_c} dx,$$

$$R_{AA'BB'} \approx \frac{\rho_{cu} * r_1}{AA'*h_c} \ln(\frac{r_2 \sin(\theta_1+\theta_2)}{r_1 \sin\theta_1})$$

Then

$$R_{AA'BB'} \approx \frac{\rho_{cu} * r_1}{(\frac{2\pi r_1}{N} - s)h_c} \ln(\frac{r_2 \sin(\theta_1+\theta_2)}{r_1 \sin\theta_1}). \quad (15)$$

For N turns (2N traces),

$$R_{Nturn} \approx \frac{2N\rho_{cu} * r_1}{(\frac{2\pi r_1}{N} - s)h_c} \ln(\frac{r_2 \sin(\theta_1+\theta_2)}{r_1 \sin\theta_1}).$$

Inserting (5), we have

$$R_{Nturn} \approx \frac{N^2 \rho_{cu}}{\pi h_c} \ln(\frac{r_2 \sin(\theta_1 + \frac{\pi}{n})}{r_1 \sin\theta_1}) \cdot \frac{1}{1 - \frac{Ns}{2\pi r_1}}, \quad (16)$$

where θ_1 and θ_2 can be calculated from (13) and (5) respectively.

From [1], the un-tilted winding resistance can be expressed as

$$R_{Nturn-untilted} \approx \frac{N^2 \rho_{cu}}{\pi h_c} \ln(\frac{r_2}{r_1}) \cdot \frac{1}{1 - \frac{Ns}{2\pi r_{ave}}}, \quad (17)$$

where r_{ave} is the average radius of the winding.

Obviously (16) is similar to (17). The use of r_1 instead of r_{ave} is just because of a different approximation while taking winding spaces into consideration. The major difference is that the inner and outer radii are O'A", O'B" respectively instead of r_1 and r_2 respectively. For θ_2=0, (16) becomes (17). As the tilt factor is defined as the resistance ratio of tilted and un-tilted windings, from (16) and (17),

$$F_{tilt} = \ln\left(\frac{r_2 \sin(\theta_1 + \frac{\pi}{n})}{r_1 \sin\theta_1}\right) / \ln\left(\frac{r_2}{r_1}\right). \qquad (18)$$

References:

[1] Zhang, Y.E.; Sanders, S.R. In-board magnetics processes. 30th Annual IEEE Power Electronics Specialists Conference. p.561-7 vol.1. 2 vol.

[2] Cheng, D.K.W.; Mo, W.K.; Lee, Y.S. Study of geometrical effects on the high frequency winding loss of low profile inductor design. Seventh International Conference on Power Electronics and Variable Speed Drives, 1998. p.405-10. xxii+679 pp.

[3] Ngo, K.D.T.; Kuo, M. H. Effect of air gaps on winding loss in high-frequency planar magnetics. 19th Annual IEEE Power Electronics Specialists Conference, Kyoto, Japan, April 1988. p.1112-19 vol.2. 2 vol. xix+1363 pp.

[4] Prieto, R.; Garcia, O.; Asensi, R.; Cobos, J.a.; Uceda, J. Optimizing the performance of planar transformers. Proceedings of Applied Power Electronics Conference. March 1996. p.415-21 vol.1. 2 vol. xviii+1003 pp.

[5] Alou, P.; Suter, O.; Cobos, A.; Uceda, J.; Ollero, S. Design of a 1.5 V output voltage on-board DC/DC converter with magnetic components integrated in a multilayer PCB. Proceedings of APEC 97 - Applied Power Electronics Conference. Feb. 1997. p.764-9 vol.2. 2 vol. xxii+1068 pp.

[6] Ramakrishnan, S.; Steigerwald, R.L.; Mallick, J.A. A comparison study of low-profile power magnetics for high-frequency, high-density switching converters. APEC '97. Twelfth Annual Applied Power Electronics Conference and Exposition. p.388-94 vol.1. 2 vol. xxii+1068 pp.

[7] Santi, E.; Cuk, S. Issues in flat integrated magnetics design. PESC Record. 27th Annual IEEE Power Electronics Specialists Conference, June 1996. p.329-35 vol.1. 2 vol. xxiv+2000 pp.

[8] Chen, W.; Hua, G.; Sable, D.; Lee, F. Design of high efficiency, low profile, low voltage converter with integrated magnetics. APEC '97. Twelfth Annual Applied Power Electronics Conference and Exposition. p.911-17 vol.2. 2 vol. xxii+1068 pp.

[9] Lotfi, A.; Van Dover, R.B.; Schneemeyer, L.; Steigerwald, M. Micro-transformer devices using thin-film electroplated deposition. PESC 98 Record. 29th Annual IEEE Power Electronics Specialists Conference. p.1511-15 vol.2. 2 vol. xxxi+2136 pp.

[10] Xu Huang; Ngo, K.D.T.; Bloom, G. Design techniques for planar windings with low resistances. APEC '95. Tenth Annual Applied Power Electronics Conference and Exposition. p.533-9 vol.2. 2 vol. (xvii+1012) pp.

[11] Mehas, G.J.; Coonley, K.D.; Sullivan, C.R. Design of microfabricated inductors for microprocessor power delivery. APEC '99. Fourteenth Annual Applied Power Electronics Conference and Exposition. p.1181-7 vol.2. 2 vol. xxx+1297 pp.

[12] Mino, M.; Yachi, T.; Yanagisawa, K.; Tago, A.; Sakakibara, K. Switching converter using thin-film microtransformer with monolithically integrated rectifier diodes. IEICE Transactions on Electronics, vol.E80-C, (no.6), Inst. Electron. Inf. & Commun. Eng, June 1997. p.821-7.

[13] Daniel, L., C.R. Sullivan, and S.R. Sanders. Design of microfabricated inductors. PESC 1996.

[14] Sullivan, C.R. and S.R. Sanders, Design of microfabricated transformers and inductors for high-frequency power conversion. IEEE Transactions on Power Electronics, 1996. 11(2): p. 228-38.

[15] Sullivan, C.R.; Sanders, S.R. Microfabrication process for high-frequency power-conversion transformers. PESC 95 Record. 26th Annual IEEE Power Electronics Specialists Conference.

[16] Clyde F. Coombs, Jr. Printed Circuits Handbook Fourth Edition. 1996, McGraw-Hill